International Journal of Bioprinting

RESEARCH ARTICLE

Printing channels with millimeter-scale curvature and deciphering their effect on the proliferation, morphology, orientation, and migration of M-22 cells

Huinan Lai[1†], Yuye Huang[2†], Jun Yin[3*], Jin Qian[1*]

[1]Department of Engineering Mechanics, Key Laboratory of Soft Machines and Smart Devices of Zhejiang Province, Zhejiang University, Hangzhou, 310027, China

[2]Center for Medical and Engineering Innovation, Central Laboratory, Ningbo First Hospital, Ningbo 315010, China

[3]The State Key Laboratory of Fluid Power Transmission and Control Systems, Key Laboratory of 3D Printing Process and Equipment of Zhejiang Province, School of Mechanical Engineering, Zhejiang University, Hangzhou 310028, China

(This article belongs to the *Special Issue: 3D Printing of Advanced Biomedical Devices*)

Abstract

Complex curved structures of tissues have been recognized to influence the behavior and function of cells. Tissue curvatures sensed by cells are approximately on the millimeter scale. However, previous research mainly focused on the effect of micro- and nano-scale spatial curved structures, underestimating the significance of milli-scale curvature. Here, we employed fused deposition modeling (FDM) with two-stage temperature control, superfine cone-shaped needle, stable air pressure, and precise motion platform for the customized production of homogeneous, precise, and curved fibers; the responses of M-22 cells to FDM-printed curved channels with radii of 1.5 to 3 mm were systematically investigated. The cells aligned with these curved channels and exhibited various aspect ratios in the channels with different curvatures. Cell proliferation, migration speed of single cells, and front-end speed of collective cells were tightly regulated by these curved structures. Also, a computational model based on force equilibrium was proposed to explore the essential factors and mechanisms of curvature affecting cell behavior. Our simulation results demonstrated that the curvature and width of channels, along with the relative size of cells, can significantly impact the cell–boundary interaction force and the number of valid pseudopodia generated by cells in the process of cell migration. These results provide a comprehensive understanding of the effect of milli-scale curvature on the cells and underpin the design of scaffolds that can be produced easily with sophisticated micro- and nano-scale curved features to regulate cell behavior in tissue engineering.

Keywords: Fused deposition modeling; Curvature effect; Curved channel; Cell behavior; Migration

[†]These authors contributed equally to this work.

***Corresponding authors:**
Jun Yin (junyin@zju.edu.cn)
Jin Qian
(jqian@zju.edu.cn)

Citation: Lai H, Huang Y, Yin J, *et al*., 2023, Printing channels with millimeter-scale curvature and deciphering their effect on the proliferation, morphology, orientation, and migration of M-22 cells. *Int J Bioprint,* 9(3): 681. https://doi.org/10.18063/ijb.681

Received: August 10, 2022
Accepted: November 8, 2022
Published Online: February 9, 2023

1. Introduction

Most native tissues contain curved architectures to maintain their mechanical and physiological function, and the curved topographic environment is expected to influence the behavior and function of the surrounding cells[1-3]. The curvature changes in the tissues have been found to lead to severe diseases, such as asthma induced by the airway narrowing[4], distorted vision due to the keratoconus bulging or flattening[5], and vertebral disorders caused by the spine bending[6]. Furthermore, the curved structures of artificial tissue engineering scaffolds can affect the behavior of seeded cells, which is crucial in clinical and biomedical applications[7-9]. Recent studies focused on the effect of micro- and nano-scale spatial curvature on cells, showing that the cellular-scale curved structures can alter the adhesion[10], orientation[11,12], migration[13,14], and gene expression[15] of cells. However, the tissue curvatures perceived by cells are also present on a millimeter scale[16]. Therefore, it is essential to probe the influence of millimeter-scale curved structures on cells.

A suitable method is required for the fabrication of millimeter-scale structures. Various methods have been employed to fabricate curved structures to guide cell behavior, including photolithography and mold[17,18]. However, the main disadvantages of photolithography and mold are high manufacturing costs and the inability to change the designed patterns. As one of the 3D printing technologies, fused deposition modeling (FDM) extrudes and deposits the melted thermoplastic materials with designed patterns layer by layer and then solidifies them by cooling[19]. The most crucial feature of FDM is that it can flexibly print the structures with desired shapes at a low cost[20]. The diameter of fibers printed by FDM was greater than 200 μm in most previous studies. For instance, Zhang *et al.* fabricated the meniscus scaffold with 300 μm diameter poly(ε-caprolactone) (PCL) fibers[21]. Ji *et al.* printed curved PCL fibers with 460–516 μm in diameter to enhance mesenchymal stem cell osteogenesis[22]. Cells can perceive the topographic structures with dimensions comparable to their own[23,24]. Two-stage temperature control, which uses two heating blocks to reconcile the flowability and formability of the thermoplastic materials, is an effective way to obtain precise and homogeneous fibers with a diameter of ~100 μm in FDM. Thus, FDM is an effective way to fabricate curved structures.

PCL has been approved by the U.S. Food and Drug Administration (FDA) as biomedical material due to its fantastic biocompatibility, biodegradability, and environmental friendliness[25,26], and it is thermoplastic and suitable for FDM printing. Therefore, PCL was chosen to form the induced patterns in the present study; siliconized glass, which adheres well to both cells and PCL, was selected as the substrate.

Several computational models have been proposed to pursue the mechanism of how curvature affects cell behavior[27]. Finite element methods used thermal stress to replicate cell contraction and calculate the direction of the maximum principal stress, which was found to be a governing factor in determining the orientation and migration of collective cells on the curved channels[28,29]. Energy minimization methods can forecast the morphology changes of cells[30,31]. In addition, cell migration can also be calculated by vertex-based methods that mesh individual cells into numerous nodes and analyze each node's migration direction and distance according to the condition of force equilibrium[32,33]. Odde's model was based on one of the vertex-based methods, which was developed to investigate the influence of substrate stiffness on cells[34]. Shih *et al.* modified Odde's model by increasing the force of cell–cell and cell–boundary interactions and making it suitable for simulating cell migration in a confined 2D space[35]. However, none of them have been used to stimulate cell behavior on curved channels.

Here, we aim to explore the effects of planar milli-scale curved channels on the cells. PCL curved structures with radii 1.5, 2, 2.5, 3, and infinite (straight) mm were printed onto the siliconized glass sheets by FDM to observe the proliferation, morphology, orientation, and migration of cells within these channels. The glass sheet without a pattern was used as a control. Our results revealed that the cells behave distinctly under the guidance of different curvatures. Also, we investigated the underlying mechanism of cellular curvature sensing observed in the experiments. A computational model based on force equilibrium was developed to simulate the migration of cells in the curved channels and served as an experiment complement to decipher the key factors in the process of cellular response to curvature. Our simulation results demonstrated that the effect of curvature on cells originated from the change in the cell–boundary interaction forces and the number of valid pseudopodia generated by the cells. Together, our findings provide a simple and effective way to manipulate cell behavior with curved channels, opening new avenues for the design of artificial tissues with desired geometric features.

2. Materials and methods

The experimental procedures for investigating the effect of curvature on cell proliferation, morphology, orientation, and migration are represented in Figure 1.

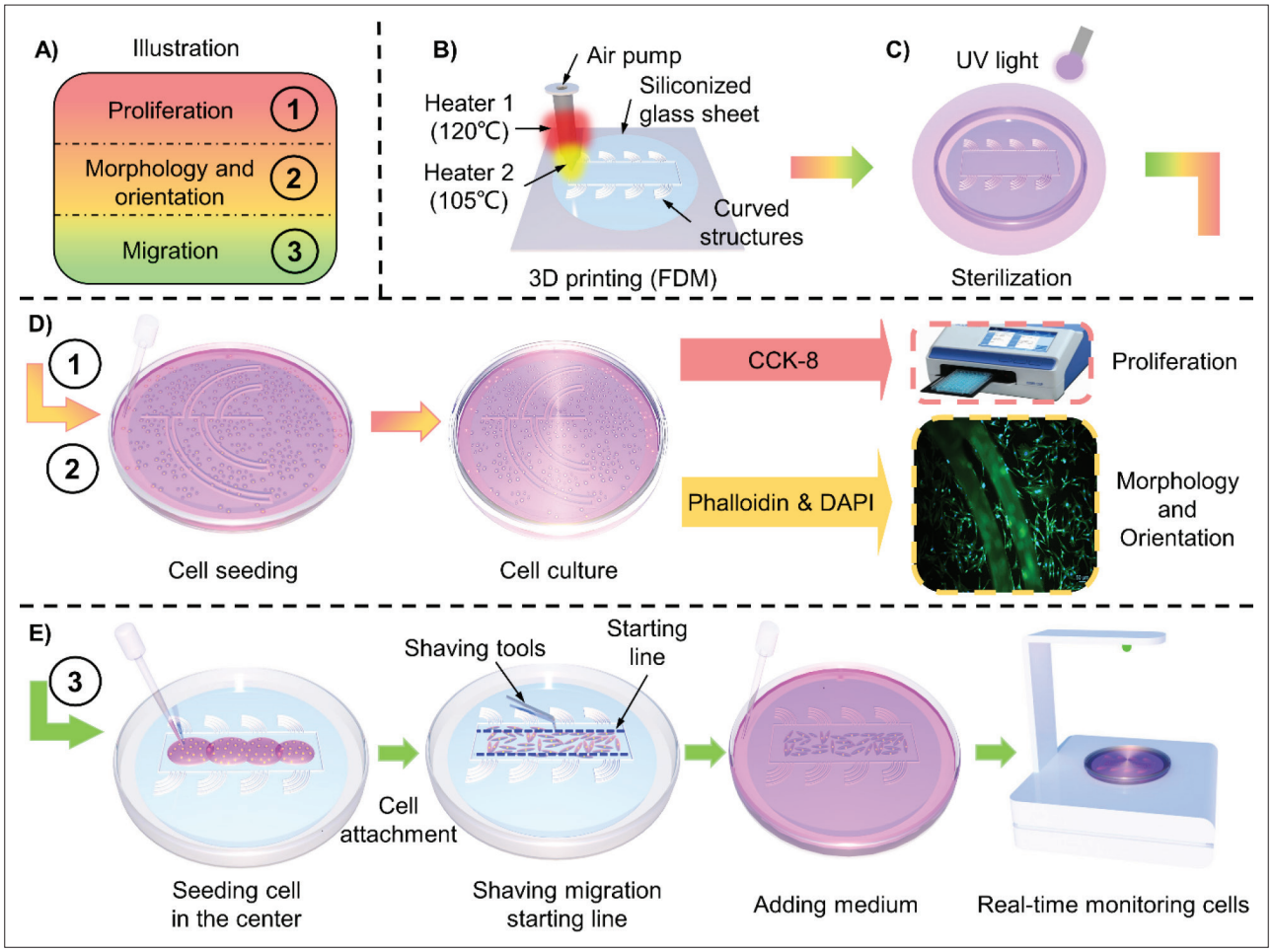

Figure 1. Schematic diagram of the fabrication of curved channels and cell culture processes. (A) Illustrative diagram of the process markers. (B) The process of printing curved channels onto the siliconized glass sheets by fused deposition modeling (FDM). (C) UV sterilization of the printed structures. (D) The observation processes of cell proliferation, morphology, and orientation observation. (E) The processes of the cell migration observation.

2.1. Curved structures fabricated by 3D printing

Medical-grade PCL (Daigang Biomaterial Co., Ltd, China) with a molecular weight of 150,000 Da was selected as the channel boundary material due to its good biocompatibility and printability. The siliconized glass sheets of 24 mm diameter (JingAn Biological Co., Ltd, China) were selected as substrate material. The siliconized glass was first fixed on the printing platform with single-sided adhesive tape before printing. The starting point of printing was selected at the center of the glass sheet. The inner diameter of the needle for structure printing was 100 μm. Two-stage temperature control was employed to heat the PCL, with the temperature being set as 120°C and 105°C, respectively. The air pressure of the printer was 0.6 MPa, and the platform movement speed was 0.8 mm/s. After the pressured air inlet was closed, the platform was configured to elevate automatically and slowly to prevent the inertia extrusion of fibers from damaging the designed structures. Predesigned channels with 100 μm in width, 150 μm in height, and 1.5, 2, 2.5, 3, and infinite (straight line) mm in radius (represented by R1.5, R2, R2.5, R3, and SL in the subsequent text) were printed by FDM onto the receiving glass sheet (Figure 1B). The size of the printed channels was observed using optical microscope (Leica, Germany), and the high-resolution surface and cross-section images of the printed fibers were observed using scanning electron microscope (Zeiss, Germany) (**Figure S1**).

2.2. Cell seeding and culture

Before cell seeding, the printed structures were placed in the culture dishes and sterilized with ultraviolet (UV) light in a UV sterilization chamber (Kangrong Biomedical Technology Co., Ltd, China) for 3 h (Figure 1C). The sterilized substrates were transferred into a clean six-well plate (JingAn Biological Co., Ltd, China).

Human embryonic fibroblast M-22 cell (M-22 cell) was spindle-shaped with a rapid migration and proliferation speed, suitable for observing the cell orientation and

migration in the curved channels[36,37]. The M-22 cells were cultured in DMEM/F12 (1:1) supplemented with 10% fetal bovine serum and 1% penicillin/streptomycin (culture medium, Gibco, US) and incubated in a humidified cell incubator (Thermo Fisher Scientific, US) at 37°C and 5% CO_2.

The cells were uniformly seeded with 10,000 and 80,000 cells per well to observe the effect of pattern curvatures on cell proliferation and morphology, respectively (Figure 1D).

For the observation of cell migration, the cells were firstly seeded in the center away from the entrance of the migration channels with 400,000 cells/mL (100 μL); after 6 h of cell adhesion, the frontier of the cell was slicked to a straight line to ensure that cells migrated from the same starting line, and then 2 mL culture medium was added to each well for continuously culturing the cells. A time-lapse microscope was used to observe the migration of cells (Figure 1E).

2.3. Cell proliferation assay

The proliferation of M-22 cells was evaluated on days 1, 2, and 4 after culturing using a cell counting kit-8 (CCK-8) (Beyotime Biotechnology Co., Ltd, China), and there were four independent replications per group. Briefly, the CCK-8 reagent was diluted (1:10) in a full culture medium as a working solution and added to each well; after 30 min, 200 μL supernatant was extracted and added to 96-well plates, this was repeated four times, and the optical density (OD) value at 450 nm was measured by a multifunction microplate reader (Thermo Fisher Scientific, US). The cell metabolism was quantified by the ratio of the OD value on day n to the average OD value on day one.

2.4. Fluorescence staining

The morphology and orientation of the cells were analyzed by fluorescence staining and microscopic observation after 48 h of incubation. Briefly, the samples were fixed in 4% paraformaldehyde (Solarbio, China) for 30 min and permeabilized with 0.5% Triton X-100 (Solarbio, China) for 20 min at room temperature. Next, the F-actin of cells was stained with 1:200 phalloidin-FITC (Solarbio, China) solution and incubated at room temperature in the dark for 2 h. Then, the cell nuclei were stained with 4',6-diamidino-2-phenylindole (DAPI) (Solarbio, China) for 10 min at room temperature in the dark. Finally, all the samples were rinsed three times with phosphate-buffered saline (PBS) and fixed on a microscope for imaging.

2.5. Characterization of cell morphology and orientation

The staining samples were observed and photographed under an inverted phase-contrast fluorescence microscope (Leica, Germany) at 10× magnification. All the cells, nearly 20 cells per group, in the channels were recorded and measured by Fiji/ImageJ (National Institute of Health, US). The morphology of cells was characterized by the aspect ratio, which was defined as the ratio of the length to width of the fitting ellipse of cells. The orientation angle of the cell was defined as the acute angle between the ellipse's major axis that fits the cells' shape and the tangent line on the pendant foot of the nucleus to the channel.

2.6. Characterization of cell migration

The front-end speed of collective cells and the migration speed of single cells were quantified as mentioned below. The front-end speed of collective cells was calculated by the ratio of the displacement of the front end of the cell population to the observation time without eliminating the influence of cell proliferation. Bright-field images were taken one day after the cells entered the channels to measure the displacement of the front end of the cell population; the time interval was 12 h.

The single-cell migration speed was defined as the average ratio of the migration distance of the cells to the observation time. The single-cell migration speed was recorded by a time-lapse microscope CytoSMART Lux2 (CytoSMART Technologies, Netherlands) after the cells entered the curved channels. Photographs were taken at 5-min intervals for 12 h. The microscopy images were imported into the Fiji/ImageJ software, the manual tracking function was used to track the displacement of 30–40 cells per channel, and the average migration speed of cells was calculated accordingly.

2.7. Computational model of cell migration

The cell migration was modeled and simulated by modifying the methods based on Odde's model[35]. The migration simulation was based on the force equilibrium between the membrane tension, cell–cell, and cell–substrate interaction force. The boundaries were set as curved, which was consistent with our experiment. The detailed model description, parameter settings, and calculation programs were described in the supporting information. The calculation programs were solved by MATLAB (Mathworks, US).

2.8. Statistical analysis

The data from the experiments are expressed in mean ± standard deviation, and the error bar represented the standard deviation of the mean value. The data were analyzed by OriginPro 2021 learning edition (OriginLab, US). The statistical significance was determined using a one-way statistical analysis of variance (ANOVA) followed by the Tukey's post-hoc test for multiple comparisons. The statistical significance was defined as * $P < 0.05$ and ** $P < 0.01$.

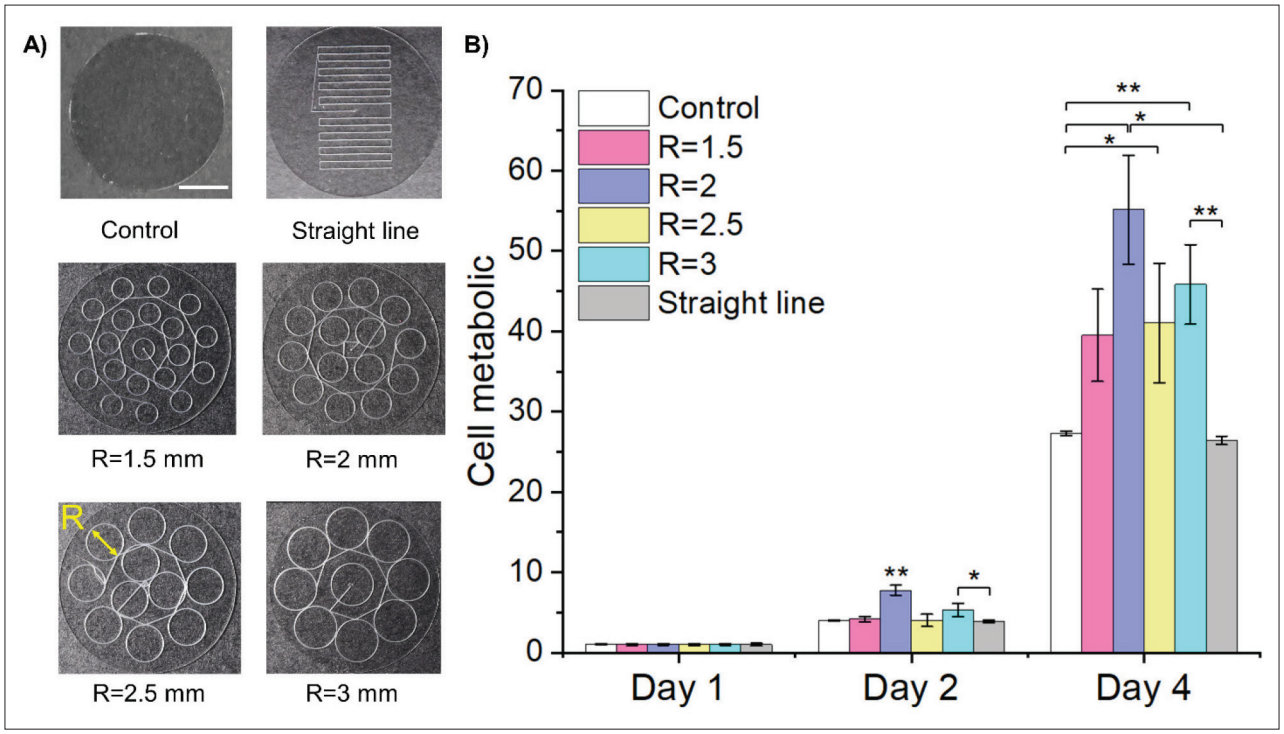

Figure 2. Cell proliferation on the patterns with varying curvature. (A) Curved structures for cell culture and proliferation test (scale bar = 10 mm). (B) The proliferation of M-22 cells (CCK-8 assay) after 1, 2, and 4 days of culture on the curved structures. The significant difference between the groups was indicated (*$P < 0.05$, **$P < 0.01$).

3. Results

3.1. Cell proliferation on curved structures

The CCK-8 test assessed cell proliferation. The structures for cell culture and proliferation test were the entire circle spreading over the entire glass sheet with the same perimeter but varying radii (Figure 2A). The cells proliferated well in all groups, indicating that the printed pattern materials and glass substrate were not toxic to cells (Figure 2B). The cell proliferation first increased and then decreased as the channel radius increased and was significantly faster in group R2 than that in the other groups on day 2 ($P < 0.01$) and day 4 ($P < 0.05$). The proliferation of groups R1.5, R2.5, and R3 showed no significant differences on day 2 and day 4. The proliferation in straight lines was approximately equal to the proliferation in control on day 2 and day 4. Notably, the cells proliferated faster in all curved groups than in the straight lines and control on day 4, where groups R2 and R3 were both significantly faster than the straight lines and control ($P < 0.05$), and group R2.5 was considerably faster than the control ($P < 0.05$).

3.2. Cell morphology and orientation in curved channels

Cell morphology was characterized by aspect ratio, which was defined as the ratio of the major axis to the minor axis of the cell fitting ellipse (Figure 3A). The smaller aspect ratio corresponds to the more rounded shape of the cells. The curved channels used to observe the morphology of cells has the same length (500π μm), width (100 μm), and depth (150 μm) (Figure 3B). The straight channel had the same width and depth as the curved groups (Figure 3C). The effect of pattern curvature on the cell morphology and orientation was evaluated after 2 days of cell seeding by analyzing the microscopic fluorescence images (Figure 3D). The aspect ratio of cells first declined and then increased as the guided radius increased, and reached the minimum in group R2. The cells were elongated in the groups R1.5, R2.5, and R3 but shortened in the groups SL and R2 compared to the control (Figure 3E). Specifically, the elongation of cells in R3 was significantly larger than that in SL ($P < 0.01$), R2 ($P < 0.01$), and control ($P < 0.05$). The elongation of cells in R1.5 was significantly greater than in SL ($P < 0.01$). Interestingly, the aspect ratio at R2 was closest to the control.

The orientation angle was employed to characterize cell orientation, which was defined as the acute angle formed by the major axis of the cell fitting ellipse and the tangent line on the pendant foot of the nucleus to the channel (Figure 3F). Cells were more oriented when the orientation angle was smaller. The distribution of cell orientation angle was uniform in the control, concentrated within 60° in the straight channels, and dispensed within 30° in the curved

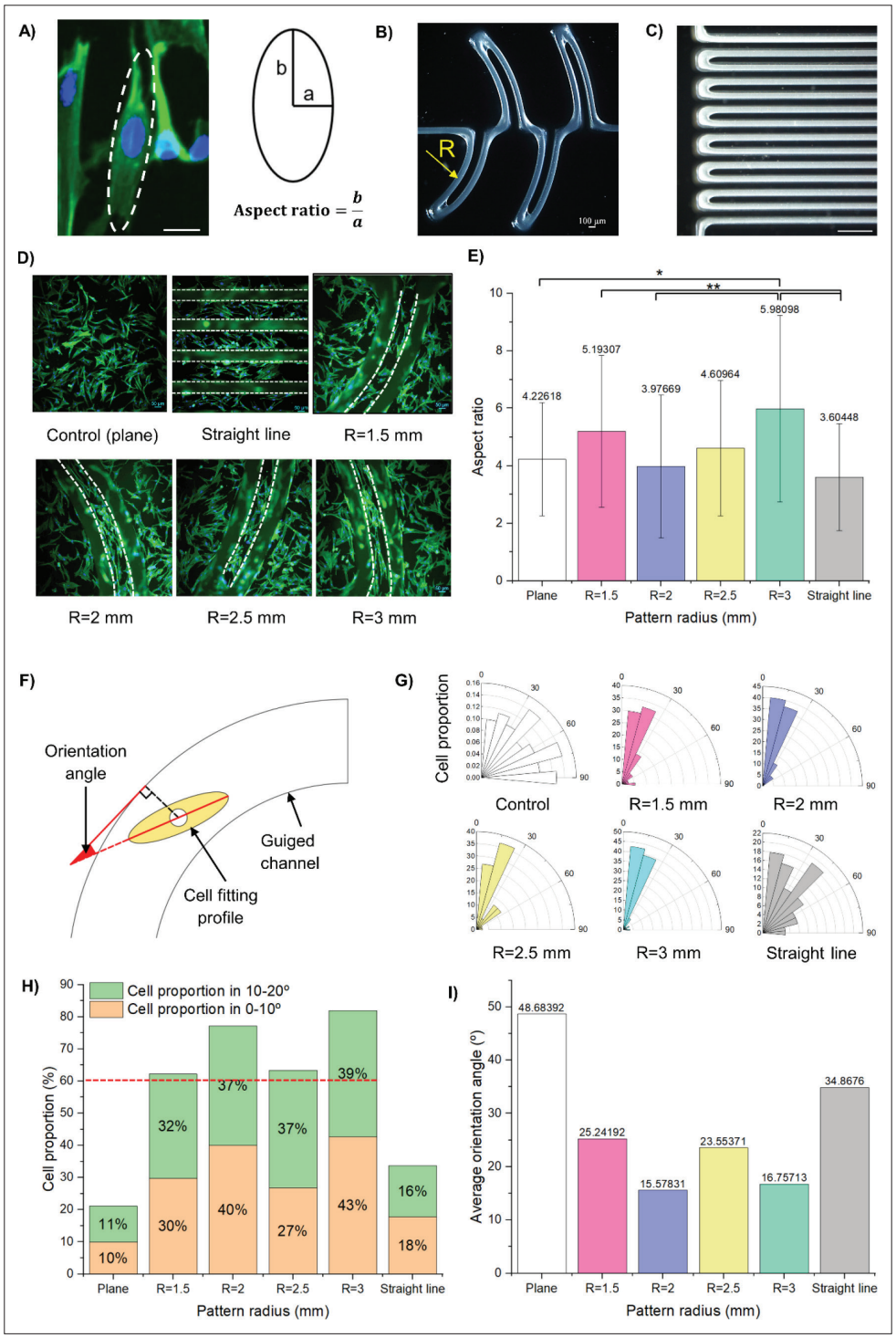

Figure 3. Cell morphology in channels with different curvatures. (A) The measurement of cell aspect ratio; a and b represent the short and long axis of the ellipse, respectively (scale bar = 20 μm). (B) Microscopic image of the curved channels for cell culture and morphology analysis (scale bar = 100 μm). (C) Microscopic image of the straight channels for cell culture and morphology analysis (scale bar = 500 μm). (D) Fluorescence images of F-actin (phalloidin, green) and nucleus (DAPI, blue) of cells on different channels (boundaries are marked in white) (scale bar = 20 μm). (E) Comparison diagram of cell aspect ratios on different curved channels after 2 days of culture. The significant difference between the investigated groups was indicated (*$P < 0.05$, **$P < 0.01$). (F) Schematic diagram of the cell orientation angle. (G) The distribution of cell orientation angles on different channels. (H) Comparison diagram of the percentage of cell orientation angle distributed in the range from 0° to 20°. (I) Comparison diagram of cell average orientation angle on different channels. The significant difference between the groups was indicated (*$P < 0.05$, **$P < 0.01$).

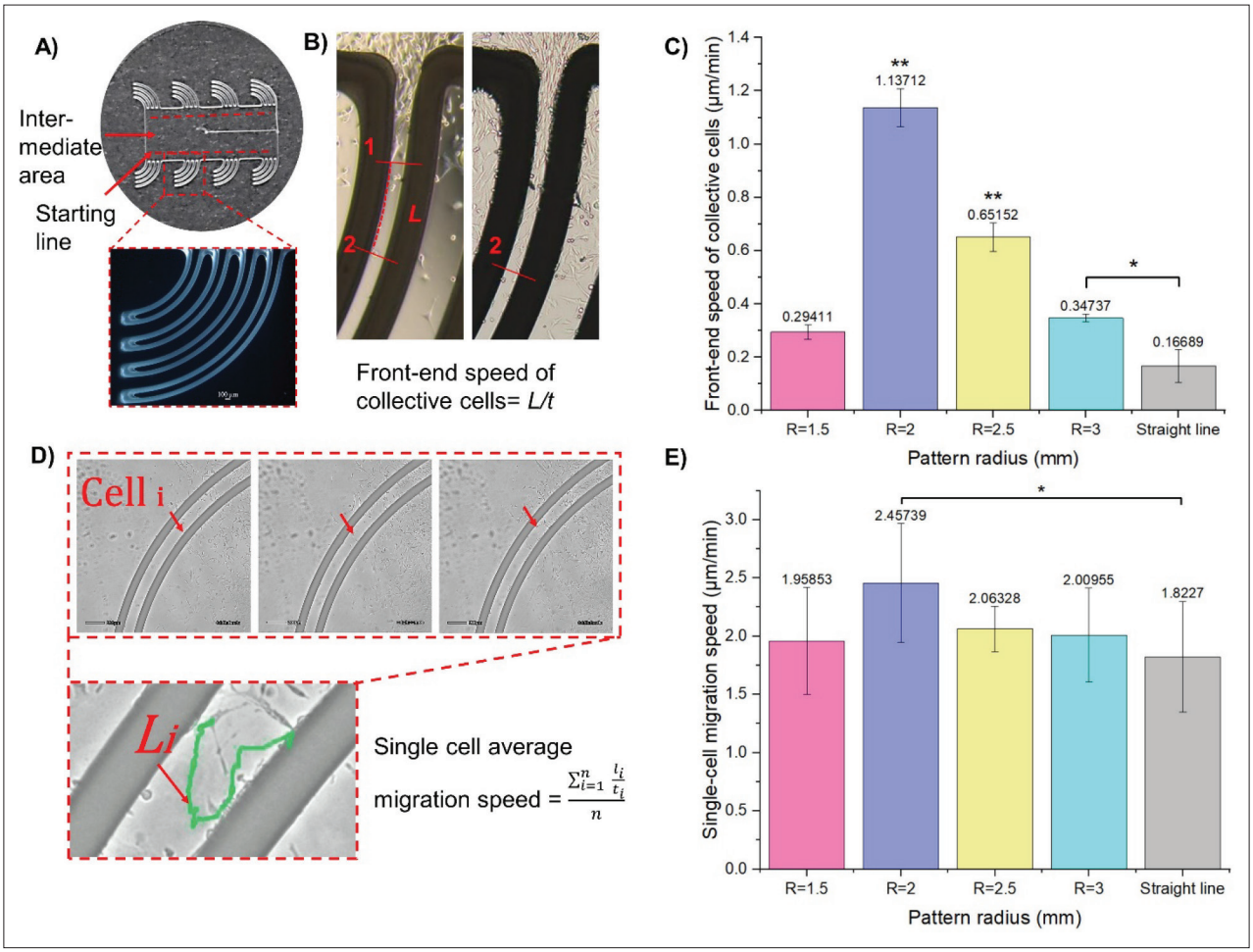

Figure 4. Cell migration in channels with varying curvatures. (A) Printed structure for observing cell migration. (B) The measurement of front-end speed of collective cells. (C) Front-end speed of collective cells in various curved channels. (D) Illustration diagram of the single-cell migration speed (n represents the number of cells counted). (E) Single-cell migration speed in various curved channels. The significant difference between the groups was indicated (*$P < 0.05$, **$P < 0.01$).

channels (Figure 3G). More than 60% of cells oriented between 0° and 20° in the curved channels, suggesting that cells aligned with the curved channels (Figure 3H). The average orientation angle was 48.68° in the control group, implying that cells oriented randomly in an unpatterned plane (Figure 3I). The average orientation angle was 34.86° in straight channels, which was close to that in control (48.68°), indicating an unremarkable orientation. The average orientation angle of all curved channels fluctuated with increasing curvature, and cells were most oriented in group R2.

3.3. Cell migration in curved channels

The structures used to observe the cell migration were composed of eight sub-regions, each sub-region contained four kinds of curvature, and the sub-regions enclosed an intermediate area that was used to unify the migration starting line (Figure 4A). Based on time-lapse images, the migration profile of the M-22 cells is described below. Cells polarized and formed tentative pseudopodia at the front to create adhesion points, and then moved the main part of the cell in the direction of the protruding pseudopod. The cells were more likely to sustain the movement in the direction they previously took than to change until they hit an obstacle or other cells.

The cell migration was characterized by the front-end speed of collective cells and the average single-cell migration speed. The front-end speed of collective cells was defined as the ratio of the displacement of the front end of the cell population (L) to the observation time (t), which did not eliminate the influence of cell proliferation (Figure 4B). The front-end speed of collective cells first increased and then decreased as the channel radii increased, reaching the maximum in R2 (Figure 4C). The R2 and R2.5 had significantly higher cell front-end speeds

than the other groups ($P < 0.01$), while the migration speed of R3 was significantly faster than SL ($P < 0.05$). The average single-cell migration speed was the average ratio of the cell migration distance (Li) to the observation time (t) (Figure 4D). The average single-cell migration speed first increased and then decreased with the increasing channel radii, reaching the maximum in R2, albeit only having a significant difference with straight channels ($P < 0.05$) (Figure 4E). Notably, the trends of the front-end speed of collective cells and single-cell migration speed with curvature were consistent, and the front-end speed of collective cells speed was smaller than the single-cell migration speed at the same curvature.

3.4. Simulation of cell migration in curved channels

The migration of cells in curved channels was simulated based on the modified Odde's model, which considered the external force generated by cell–boundary and cell–cell interactions (F_{ext}), the force acting on the cell body from the substrate (F_{cell}), the force acting on modules from the substrate (F_{mod}), and membrane tension (F_{mem}), with force balance in Cartesian coordinates to calculate cell migration (Figure 5A). The adhesion proteins (fibronectin) were strained to ensure that the external force generated by cell–boundary and cell–cell interactions was exist (**Figure S2**).

First, the migration of cells in curved and straight channels with a width of 100 μm was simulated and compared to the experimental results to estimate the model's applicability. The magnitude of the migration speed of all groups in the simulation was close to the speed of the experiment, and the trend of change in migration speed with curvature was also consistent with the experimental findings, indicating that the model can accurately describe the migration of cells in the curved channels (Figure 5B).

Subsequently, the cell migration in the channels with different widths (D = 50, 100, 150, and 200 μm) and various radii (R = 1.5, 2, 2.5, 3, and infinite mm) was simulated. Interestingly, the maximum migration speed was observed at various radii when the width of channels was different. The cell migrated the fastest at R1.5 when the channel width was 200 μm, but migrated fastest at R2 when the channel width was 150, 100, and 50 μm. The radius corresponding to the maximum migration speed increased as the channel width decreased, implying that the width of the induced channel and the relative size of the cells affected the migration speed of cells in the channels with the same curvature. Moreover, the migration speed was increased with a decrease in channel width at the same curvature, which was consistent with the experiment in reference[38].

Furthermore, the mechanism by which curvature affected cell behavior was explored. We observed and investigated the process of cell migration in the experiment. Cells polarize and form tentative pseudopodia at the front to create adhesion points during migration[39]. When a cell encounters a boundary that cannot cross, it will retract the original pseudopodia and form a new one in the other direction to change the migration direction due to the force between the cell and the channel wall. Therefore, we inferred that the curvature mainly influenced the force of cell–boundary interaction and the number of invalid pseudopodia (need to retract and form a new one) to regulate the cell behavior (Figure 5C). The forces generated from cell–boundary interaction were proportional to the area of the cell intersecting the boundary. The invalid pseudopodia were generated from the node of the cell perimeter within the boundary. Therefore, the accumulative intersection area and the number of invalid pseudopodia were recorded during the simulation, and their correlation with cell migration speed was analyzed to prove the hypothesis. The results showed that the accumulative intersection area was positively linear and correlated with cell migration speed (Figure 5D). The number of invalid modules was negatively allometric correlated with the cell migration speed (Figure 5E), indicating that our hypothesis was accurate.

Altogether, the abovementioned results demonstrated that the M-22 cells can sense and respond to curved structures with curvature on the millimeter scale.

4. Discussion

Most cells grow in a curved topographic environment that can impact their behavior and function. Meanwhile, the structures of the curved scaffolds can affect the activities of the seeded cells, which is crucial for the success of tissue engineering. The curvatures at the organ level (millimeter scale) sensed by cells are approximately planar. However, most of the research was concentrated on the effect of micro- and nano-scale spatial curvature on cells, underestimating the importance of milli-scale planar curvatures. In this study, planar channels with 1.5, 2, 2.5, 3, and infinity (straight line) mm in radius, 100 μm in width, and 150 μm in depth were printed on the silicide glass sheets to investigate the effect of planar milli-scale curvature on the proliferation, morphology, orientation, and migration of the spindle cells (M-22 cells). We demonstrated that the curved channels had a more significant impact on the cells than straight channels, with differences between the curved groups. The cell proliferation and migration speed first increased and then decreased with increasing channel radius, reaching a maximum in group R2. The cells were first round in shape and then elongated as the radius increased, and were roundest at R2. The orientation angle fluctuated with increasing radius, and cells were the

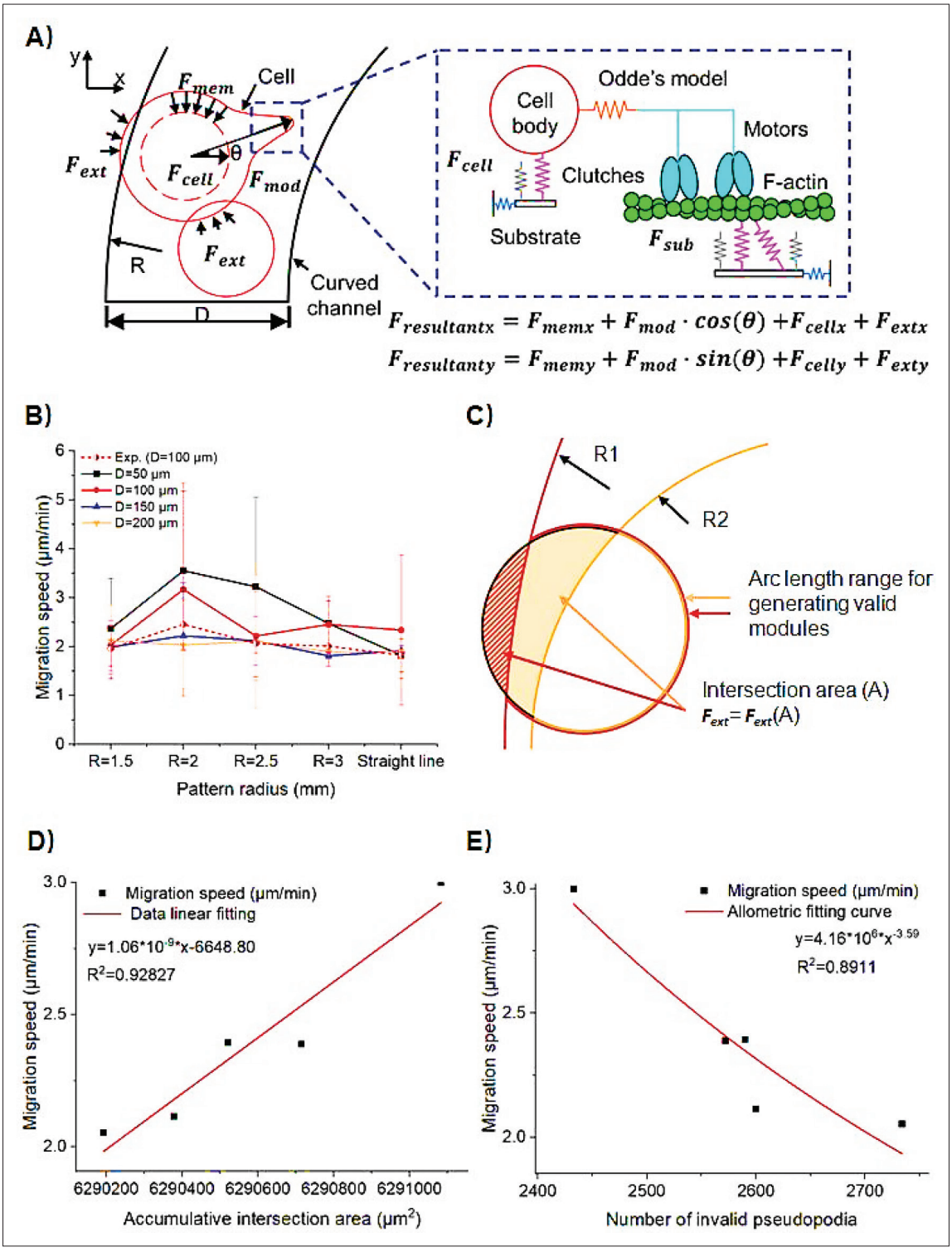

Figure 5. (A) A computational model of cell migration. (B) Simulation results of cell migration speed in curved channels with different widths (50, 100, 150, and 200 μm) and different radii (1.5, 2, 2.5, 3, and infinite mm), which were consistent with the experiment data (dash line). (C) The mechanism of curvature affects the cell migration speed. (D) Correlation analysis diagram of the relationship between migration speed and accumulative intersecting cell–boundary area. (E) Correlation analysis diagram of the relationship between migration speed and the number of invalid pseudopodia.

most oriented at R2. Also, a computational model was employed to explore the mechanism of the experimental phenomenon. The results showed that the curvature effect on the cells was mainly caused by the influence of the cell–boundary interaction forces and the invalid number of pseudopods generated by the cells.

4.1. The interplay between proliferation, shape, and migration of cells

It should be noted that the changes in cell morphology and single-cell migration speed under the influence of curvature were relevant. Previous studies and our time-lapse videos (**Videoclips S1–3**) proved that cells extend their lamellipodia while migrating[40]. When a cell extends its lamellipodia, the cell body lays flat, causing the aspect ratio to decrease. In addition, the morphology was also related to cell proliferation. After analyzing the videos (**Videoclips S1–3**), we discovered that the cytoplasm shrinks inward first, and the cell takes on a spherical shape before dividing. Other studies also confirmed the transformation of cell morphology in the proliferation process[41]. The faster the proliferation and migration speed, the higher the probability of staining the dividing and migrating cells.

In addition, although the trend of the front-end speed of collective cells with channel curvature coincided with single-cell migration speed, the magnitude of the front-end speed of collective cells was lower than the single-cell migration speed in all groups. The stochastic cell migration direction could explain the results; namely, cells will move forward, backward, or perpendicular to the channels randomly, but the front-end speed of collective cells only considers the cells that migrated forward (Figure 4D). Moreover, the difference value of the magnitude of the front-end speed of collective cells and single-cell migration speed in various curvatures was varied. One of the reasons was that the front-end speed of collective cells included cell proliferation, which was also influenced by curvature and could compensate for the effects of random cell migration. Another possible reason was that curvature could affect the proportion of cells moving forward, backward, and perpendicular to the channels during migration, which can be verified in the study's next step.

4.2. Effect of channel width on cell's response to curvature

The influence of channels with different widths (200, 150, 100, and 50 μm), different radii (1.5, 2, 2.5, 3, and infinite mm), and the same cell diameter (20 μm) was compared in the simulation, which demonstrated that the migration speed increased as the channel width decreased regardless of the curvature (**Videoclips S4–8**). Besides, the maximum migration speed was observed at R1.5, R2, R2, and R2 when the channel width was 200, 150, 100, and 50 μm, respectively. The above findings suggested that channel width was a crucial factor affecting the cellular response to the same curvature. Similar research that cultured cells on circular annulus grooves with 100, 150, and 200 μm in width confirmed this concept, and showed that the narrower the channels, the cells were more aligned along the channels[13]. However, a study concluded that the MC3T3-E1 cells oriented at curved channels with 50, 100, 150, and 200 μm in radii only due to the width of the induction channel, but independent of curvature[42]. In our experiments and simulations, a significant difference between the curved and straight channels was not observed until the width of the channel was ten times (200 μm) the width of cells, which indicated that the millimeter-scale curvature could influence the behaviors of cells within a specific range of channel width.

The possible reason for this effect is that the proportion of cells directly in contact with the curved channel is various, and a greater fraction of cells interact directly with the curved channel wall in the narrower channel. Some studies proposed the entropy effect of lateral confinement, which contained the entropy of mixing between packets of unbound and bound stress fiber proteins with sites for bound proteins, and the entropy of mixing between unbound proteins and lattice sites, to explain why cells behave differently on the channel with different width[43]. In our experiment, stress fibers evolve between bound and unbound states in the process of cell migration; therefore, the entropy effect of confinement also existed in our experiment, and this made the interpretation more complex.

4.3. Underlying mechanism of millimeter-scale curvature on the cells

Previous studies demonstrated that cell behavior was changed by the topographic cues due to the changes in cell stress, which can activate the signal molecules and pathways of cells[44]. For instance, the compressive force can increase the expression of miR-494-3p in the MC3T3-E1 cells to inhibit cell proliferation[45]. Contrarily, tension stress facilitates the cell proliferation of the epidermal cell[46]. Moreover, the cells align along with the direction of maximum shearing stress[4], and the migration is intrinsically motivated by force[29]. Therefore, many force- and energy-based simulation methods, such as self-propelled particles, cellular Potts models, and vertex-based approaches, have been developed[27]. Our model was a vertex-based approach, which was modified based on Odde's model. The simulation results showed that the curvature influenced the cell migration by affecting the cell–boundary interaction force and the number of valid pseudopodia. However, this approach simplified the cell–cell and cell–boundary interactions to elastic collision, but

the actual interactions are far more complicated. Cellular interactions include not only mechanical forces but a series of signal transformations[47,48].

Moreover, recent research showed that cells tend to leave long-lived physicochemical footprints along their migration trajectories, which can alter the path of themselves and other cells[49]. This phenomenon should be transformed into a mathematical description and considered in a model in the future. Besides, the cells were regarded as a circle in this model, which did not correspond to spindle cells in the experiment and caused inaccuracy between the experiment and the simulation.

4.4. Effect of curvature ranging from nano-scale to milli-scale on the cells

Curvatures can influence the cell's behavior on the nanometer to the millimeter scale. The curved structures at the supracellular scale only directly affect the cells near the curved pattern and indirectly impact the farther cells via cell–cell interactions[50]. Subcellular or cellular-scale curvature can directly contact and impact the cells[5].

Supracellular curvature can affect the cell's behavior, especially in cell migration. Myoblasts migrated parallel to the longitudinal direction of the hemicylinder-shaped non-planar surfaces with diameters of 3–50 mm, and cell differentiation and orientation were also augmented on the surfaces[11]. In this study, we investigated the effect of curved channels with radii of 1.5–3 mm on cell proliferation, morphology, orientation, and migration, with the results showing that the curvature can influence the aforementioned cell behaviors in this range. The curvature slightly larger than cells (tens to hundreds of microns) can facilitate the alignment of cells[51,52] and change the migration trajectories and speed[53,54].

Curvatures at the cellular scale (a few microns to a dozen microns) can impact cell behavior, particularly can directly change the morphology and distribution of the cells. Cells avoided convex regions when migrating, and positioned themselves in concave valleys (radius: 1–30 μm, period: 10, 30, and 100 μm)[55]. Similar research showed that the convex regions (radius: 10 μm, period: 100 μm) acted as topographical barriers to control the organization of the actin cytoskeleton and nuclei, as well as the collective migration and orientation of cells[56].

Subcellular scale curves mainly regulate the spreading area, orientation, and migration speed of cells. Grooved substrates with radii ranging from 10 to 400 nm can increase the spreading area of the mouse embryonic fibroblasts, but reduce their polarization (aspect ratio) when the radius increased to 200 nm[57]. Only weak impact was put on the cell spreading area and polarization when the radius was 200 and 400 nm. Fibers with 50–2000 nm in diameter can influence the migration speed of mouse mesenchymal stem cells, and the maximum migration speed was observed with the fibers with 800 nm diameter[58].

Interestingly, the cells are mainly directed by one of the curvatures when two different scales of curvature guide the cells simultaneously. Research has shown that mesoscale curvature can overrule the influence of nanoscale curvature[59]. Cell alignment and migration were governed by the nano-scale fibers (diameter: 100–200 nm) when the curvatures of the cylindrical surfaces were low (diameter > 1000 μm), and the cells increasingly aligned and migrated along the axis of the cylindrical surface as the surface diameter decreased (diameter: 250–1000 μm).

5. Conclusion

In this study, channels with customized curvature and width were printed using a two-stage temperature-controlled FDM method, and the effect of millimeter-scale curvature of curved channels on the proliferation, morphology, orientation, and migration of M-22 cells was systematically investigated *in vitro*. The experimental results indicated that the cells significantly changed their morphology and aligned along with the curved channels; the proliferation, single-cell, and front-end speed of collective cells were all increased on these curved structures, compared with the straight and unstructured counterparts. Moreover, the migration of cells in curved channels with varying widths and radii was numerically simulated, with the results showing that the channel width and relative size of the cells could influence their response to curvature. Our simulation results also demonstrated the mechanism involved, i.e., curved channels can affect the cell–boundary interaction force and the number of valid pseudopodia to regulate the cell behavior. Our findings proved that the cells could sense and respond to planar millimeter-scale curvatures and revealed the underlying mechanism of this phenomenon. To the best of our knowledge, this is the first time that the effect of planar milli-scale curvature on the cells has been explored. It provides a practical and straightforward way to manipulate cell behavior with millimeter-scale features rather than manufacturing expensive and complex micro-and nano-patterns. The finding mentioned above, wherein milli-scale curvature can promote the proliferation, orientation, and migration speed of cells, can be applied to the design of tissue scaffolds and facilitate tissue repair in the future.

Acknowledgments

We would like to thank Professor Po-Jen Shih of National Taiwan University for answering our questions on the computational model of cell migration.

Funding

This work was supported by the National Natural Science Foundation of China (Grant Numbers: 12125205, 12072316, 12132014, and 52075482), the Key Research and Development Program of Zhejiang Province (2021C01183), and the Zhejiang Provincial Natural Science Foundation of China (LD22A020001).

Conflict of interest

The authors declare no conflict of interests.

Author contributions

Conceptualization: Huinan Lai, Yuye Huang, Jun Yin, Jin Qian
Investigation: Huinan Lai, Jun Yin, Jin Qian
Methodology: Huinan Lai, Yuye Huang, Jun Yin, Jin Qian
Writing – original draft: Huinan Lai
Writing – review & editing: Yuye Huang, Jun Yin, Jin Qian

Ethics approval and consent to participate

Not applicable.

Consent for publication

Not applicable.

Availability of data

Not applicable.

References

1. Huang C-K, Paylaga GJ, Bupphathong S, *et al.*, 2020, Spherical microwell arrays for studying single cells and microtissues in 3D confinement. *Biofabrication*, 12(2):025016.

   https://doi.org/10.1088/1758-5090/ab6eda

2. Callens SJP, Uyttendaele RJC, Fratila-Apachitei LE, *et al.*, 2020, Substrate curvature as a cue to guide spatiotemporal cell and tissue organization. *Biomaterials*, 232:119739.

   https://doi.org/10.1016/j.biomaterials.2019.119739

3. Altay G, Tosi S, García-Díaz M, *et al.*, 2020, Imaging the cell morphological response to 3D topography and curvature in engineered intestinal tissues. *Front Bioeng Biotechnol*, 8:294.

   https://doi.org/10.3389/fbioe.2020.00294

4. An SS, Bai TR, Bates JHT, *et al.*, 2007, Airway smooth muscle dynamics: A common pathway of airway obstruction in asthma. *Eur Respir J*, 29(5):834–860.

   https://doi.org/10.1183/09031936.00112606

5. Baptista D, Teixeira L, van Blitterswijk C, *et al.*, 2019, Overlooked? Underestimated? Effects of substrate curvature on cell behavior. *Trends Biotechnol*, 37(8):838–854.

   https://doi.org/10.1016/j.tibtech.2019.01.006

6. Vutan A-M, Ciupe V, Gruescu CM, *et al.*, 2018, Experimental method for dynamic evaluation of spinal column deformation exercises. in *New Advances in Mechanism and Machine Science*, Springer, 137–146.

   https://doi.org/10.1007/978-3-319-79111-1_13

7. Yang C-Y, Huang W-Y, Chen L-H, *et al.*, 2021, Neural tissue engineering: The influence of scaffold surface topography and extracellular matrix microenvironment. *J Mater Chem B*, 9(3):567–584.

   https://doi.org/10.1039/d0tb01605e

8. Lai H, Gong B, Yin J, *et al.*, 2022, 3D printing topographic cues for cell contact guidance: A review. *Mater Des*, 218:110663.

   https://doi.org/10.1016/j.matdes.2022.110663

9. Li H, Xu Y, Xu H, *et al.*, 2014, Electrospun membranes: Control of the structure and structure related applications in tissue regeneration and drug delivery. *J Mater Chem B*, 2(34):5492–5510.

   https://doi.org/10.1039/c4tb00913d

10. Assoian RK, Bade ND, Cameron CV, *et al.*, 2019, Cellular sensing of micron-scale curvature: A frontier in understanding the microenvironment. *Open Biol*, 9(10):190155.

    https://doi.org/10.1098/rsob.190155

11. Wan LQ, Ronaldson K, Park M, *et al.*, 2011, Micropatterned mammalian cells exhibit phenotype-specific left-right asymmetry. *Proc Natl Acad Sci*, 108(30):12295–12300.

    https://doi.org/10.1073/pnas.1103834108

12. Mao M, He J, Li Z, *et al.*, 2020, Multi-directional cellular alignment in 3D guided by electrohydrodynamically-printed microlattices. *Acta Biomater*, 101:141–151.

    https://doi.org/10.1016/j.actbio.2019.10.028

13. Ray A, Lee O, Win Z, *et al.*, 2017, Anisotropic forces from spatially constrained focal adhesions mediate contact guidance directed cell migration. *Nat Commun*, 8(1):1–17.

    https://doi.org/10.1038/ncomms14923

14. Bade ND, Xu T, Kamien RD, *et al.*, 2018, Gaussian curvature directs stress fiber orientation and cell migration. *Biophys J*, 114(6):1467–1476.

    https://doi.org/10.1016/j.bpj.2018.01.039

15. Chao PG, Hsu H-Y, Tseng H-Y, 2014, Electrospun microcrimped fibers with nonlinear mechanical properties enhance ligament fibroblast phenotype. *Biofabrication*, 6(3):035008.

    https://doi.org/10.1088/1758-5082/6/3/035008

16. Connon CJ, Gouveia RM, 2021, Milliscale substrate curvature promotes myoblast self-organization and differentiation. *Adv Biol*, 5(4):2000280.

    https://doi.org/10.1002/adbi.202000280

17. Son J, Bang MS, Park JK, 2019, Hand-maneuverable collagen sheet with micropatterns for 3D modular tissue engineering. *ACS Biomater Sci Eng*, 5(1):339–345.

    http://doi.org/10.1021/acsbiomaterials.8b01066

18. Carthew J, Taylor JBJ, Garcia-Cruz MR, *et al.*, 2021, The bumpy road to stem cell therapies: Rational design of surface topographies to dictate stem cell mechanotransduction and fate. *ACS Appl Mater Interfaces*, 14(20):23066–23101.

    https://doi.org/10.1021/acsami.1c22109

19. Mei Y, He C, Gao C, *et al.*, 2021, 3D-printed degradable anti-tumor scaffolds for controllable drug delivery. *Int J Bioprinting*, 7(4):418.

    https://doi.org/10.18063/ijb.v7i4.418

20. Saha SK, Wang D, Nguyen VH, *et al.*, 2019, Scalable submicrometer additive manufacturing. *Science (80-)*, 366(6461):105–109.

    https://doi.org/10.1126/science.aax8760

21. Zhang Z-Z, Wang S-J, Zhang J-Y, *et al.*, 2017, 3D-printed poly (ε-caprolactone) scaffold augmented with mesenchymal stem cells for total meniscal substitution: A 12- and 24-week animal study in a rabbit model. *Am J Sports Med*, 45(7):1497–1511.

    https://doi.org/10.1177/0363546517691513

22. Ji S, Guvendiren M, 2019, 3D printed wavy scaffolds enhance mesenchymal stem cell osteogenesis. *Micromachines*, 11(1):31.

    https://doi.org/10.3390/mi11010031

23. Hou Y, Xie W, Yu L, *et al.*, 2020, Surface roughness gradients reveal topography-specific mechanosensitive responses in human mesenchymal stem cells. *Small*, 16(10):1905422.

    https://doi.org/10.1002/smll.201905422

24. Nguyen AT, Sathe SR, Yim EKF, 2016, From nano to micro: Topographical scale and its impact on cell adhesion, morphology and contact guidance. *J Phys Condens Matter*, 28(18):183001.

    https://doi.org/10.1088/0953-8984/28/18/183001

25. Buyuksungur S, Tanir TE, Buyuksungur A, *et al.*, 2017, 3D printed poly (ε-caprolactone) scaffolds modified with hydroxyapatite and poly (propylene fumarate) and their effects on the healing of rabbit femur defects. *Biomater Sci*, 5(10):2144–2158.

    https://doi.org/10.1039/c7bm00514h

26. Hedayati SK, Behravesh AH, Hasannia S, *et al.*, 2020, 3D printed PCL scaffold reinforced with continuous biodegradable fiber yarn: A study on mechanical and cell viability properties. *Polym Test*, 83106347.

    https://doi.org/10.1016/j.polymertesting.2020.106347

27. Buttenschön A, Edelstein-Keshet L, 2020, Bridging from single to collective cell migration: A review of models and links to experiments. *PLoS Comput Biol*, 16(12):e1008411.

    https://doi.org/10.1371/journal.pcbi.1008411

28. Du W, Chen J, Li H, *et al.*, 2016, Direct cellular organization with ring-shaped composite polymers and glass substrates for urethral sphincter tissue engineering. *J Mater Chem B*, 4(22):3998–4008.

    https://doi.org/10.1039/c6tb00437g

29. Zhao J, Manuchehrfar F, Liang J, 2020, Cell–substrate mechanics guide collective cell migration through intercellular adhesion: A dynamic finite element cellular model. *Biomech Model Mechanobiol*, 19(5):1781–1796.

    https://doi.org/10.1007/s10237-020-01308-5

30. Albert PJ, Schwarz US, 2014, Dynamics of cell shape and forces on micropatterned substrates predicted by a cellular Potts model. *Biophys J*, 106(11):2340–2352.

    https://doi.org/10.1016/j.bpj.2014.04.036

31. McEvoy E, Deshpande VS, McGarry P, 2017, Free energy analysis of cell spreading. *J Mech Behav Biomed Mater*, 74:283–295.

    https://doi.org/10.1016/j.jmbbm.2017.06.006

32. Kim M-C, Kim C, Wood L, *et al.*, 2012, Integrating focal adhesion dynamics, cytoskeleton remodeling, and actin motor activity for predicting cell migration on 3D curved surfaces of the extracellular matrix. *Integr Biol*, 4(11):1386–1397.

    https://doi.org/10.1039/c2ib20159c

33. Kim M-C, Neal DM, Kamm RD, *et al.*, 2013, Dynamic modeling of cell migration and spreading behaviors on fibronectin coated planar substrates and micropatterned geometries. *PLoS Comput Biol*, 9(2):e1002926.

    https://doi.org/10.1371/journal.pcbi.1002926

34. Bangasser BL, Shamsan GA, Chan CE, *et al.*, 2017, Shifting the optimal stiffness for cell migration. *Nat Commun*, 8(1):1–10.

    https://doi.org/10.1038/ncomms15313

35. Chang C, Dai Z, Shih P, 2022, Modeling and simulation of cell migration on the basis of force equilibrium. *Int J Numer Method Biomed Eng*, 38(2):e3550.

    https://doi.org/10.1002/cnm.3550

36. Zhang J, Gao Z, Zhang Y, *et al.*, 2020, Study on chitosan-based nanocomposite hydrogel in soft tissue defect of hand. *Nanosci Nanotechnol Lett*, 12(9):1120–1126.

    https://doi.org/10.1166/nnl.2020.3217

37. Ge L, Yang L, Bron R, *et al.*, 2020, Topography-mediated fibroblast cell migration is influenced by direction, wavelength, and amplitude. *ACS Appl Bio Mater*, 3(4):2104–2116.

    https://doi.org/10.1021/acsabm.0c00001

38. Vedula SRK, Leong MC, Lai TL, *et al.*, 2012, Emerging modes of collective cell migration induced by geometrical constraints. *Proc Natl Acad Sci*, 109(32):12974–12979.

    https://doi.org/10.1073/pnas.1119313109

39. Seetharaman S, Etienne-Manneville S, 2020, Cytoskeletal crosstalk in cell migration. *Trends Cell Biol*, 30(9):720–735.

    https://doi.org/10.1016/j.tcb.2020.06.004

40. Innocenti M, 2018, New insights into the formation and the function of lamellipodia and ruffles in mesenchymal cell migration. *Cell Adh Migr*, 12(5):401–416.

    https://doi.org/10.1080/19336918.2018.1448352

41. Moussa HI, Chan WY, Logan M, *et al.*, 2020, Limitation in controlling the morphology of mammalian vero cells induced by cell division on asymmetric tungsten-silicon oxide nanocomposite. *Materials (Basel)*, 13(2):335.

    https://doi.org/10.3390/ma13020335

42. He S, Liu C, Li X, *et al.*, 2015, Dissecting collective cell behavior in polarization and alignment on micropatterned substrates. *Biophys J*, 109(3):489–500.

    https://doi.org/10.1016/j.bpj.2015.06.058

43. Buskermolen ABC, Ristori T, Mostert D, *et al.*, 2020, Cellular contact guidance emerges from gap avoidance. *Cell Rep Phys Sci*, 1(5):100055.

    https://doi.org/10.1016/j.xcrp.2020.100055

44. Liu C, Xu J, He S, *et al.*, 2018, Collective cell polarization and alignment on curved surfaces. *J Mech Behav Biomed Mater*, 88:330–339.

    https://doi.org/10.1016/j.jmbbm.2018.08.014

45. Iwawaki Y, Mizusawa N, Iwata T, *et al.*, 2015, MiR-494-3p induced by compressive force inhibits cell proliferation in MC3T3-E1 cells. *J Biosci Bioeng*, 120(4):456–462.

    https://doi.org/10.1016/j.jbiosc.2015.02.006

46. Pietramaggiori G, Liu P, Scherer SS, *et al.*, 2007, Tensile forces stimulate vascular remodeling and epidermal cell proliferation in living skin. *Ann Surg*, 246(5):896–902.

    https://doi.org/10.1097/SLA.0b013e3180caa47f

47. SenGupta S, Parent CA, Bear JE, 2021, The principles of directed cell migration. *Nat Rev Mol Cell Biol*, 22(8): 529–547.

    https://doi.org/10.1038/s41580-021-00366-6

48. Yamada KM, Sixt M, 2019, Mechanisms of 3D cell migration. *Nat Rev Mol Cell Biol*, 20(12):738–752.

    https://doi.org/10.1038/s41580-019-0172-9

49. D'alessandro J, Cellerin V, Benichou O, *et al.*, 2021, Cell migration guided by long-lived spatial memory. *Nat Commun*, 12(1):1–10.

    https://doi.org/10.1038/s41467-021-24249-8

50. Haeger A, Wolf K, Zegers MM, *et al.*, 2015, Collective cell migration: Guidance principles and hierarchies. *Trends Cell Biol*, 25(9):556–566.

    https://doi.org/10.1016/j.tcb.2015.06.003

51. Xi W, Sonam S, Beng Saw T, *et al.*, 2017, Emergent patterns of collective cell migration under tubular confinement. *Nat Commun*, 8(1):1–15.

    https://doi.org/10.1038/s41467-017-01390-x

52. van Der Putten C, Buskermolen ABC, Werner M, *et al.*, 2021, Protein micropatterning in 2.5 D: An approach to investigate cellular responses in multi-cue environments. *ACS Appl Mater Interfaces*, 13(22):25589–25598.

    https://doi.org/10.1021/acsami.1c01984

53. Werner M, Petersen A, Kurniawan NA, *et al.*, 2019, Cell-perceived substrate curvature dynamically coordinates the direction, speed, and persistence of stromal cell migration. *Adv Biosyst*, 3(10):1900080.

    https://doi.org/10.1002/adbi.201900080

54. Werner M, Blanquer SBG, Haimi SP, *et al.*, 2017, Surface curvature differentially regulates stem cell migration and differentiation via altered attachment morphology and nuclear deformation. *Adv Sci*, 4(2):1600347.

    https://doi.org/10.1002/advs.201600347

55. Pieuchot L, Marteau J, Guignandon A, *et al.*, 2018, Curvotaxis directs cell migration through cell-scale curvature landscapes. *Nat Commun*, 9(1):1–13.

    https://doi.org/10.1038/s41467-018-06494-6

56. Rougerie P, Pieuchot L, Dos Santos RS, *et al.*, 2020, Topographical curvature is sufficient to control epithelium elongation. *Sci Rep*, 10(1):1–14.

    https://doi.org/10.1038/s41598-020-70907-0

57. Mathur A, Moore SW, Sheetz MP, *et al.*, 2012, The role of feature curvature in contact guidance. *Acta Biomater*, 8(7):2595–2601.

    https://doi.org/10.1016/j.actbio.2012.03.025

58. Bowers DT, Brown JL, 2021, Nanofiber curvature with Rho GTPase activity increases mouse embryonic fibroblast random migration velocity. *Integr Biol*, 13(12):295–308.

    https://doi.org/10.1093/intbio/zyab022

59. Werner M, Kurniawan NA, Korus G, *et al.*, 2018, Mesoscale substrate curvature overrules nanoscale contact guidance to direct bone marrow stromal cell migration. *J R Soc Interface*, 15(145):20180162.

    https://doi.org/10.1098/rsif.2018.0162